Electronic Supplementary Information

A BODIPY Small Molecule as Hole Transporting Material for Efficient Perovskite Solar Cells

John Marques Dos Santos,[a¶] Lethy Krishnan Jagadamma,[b¶] Michele Cariello,[a] Ifor D. W. Samuel,[b*] Graeme Cooke[a*]

[a.] *WestCHEM, School of Chemistry, University of Glasgow, Glasgow, G12 8QQ, UK.*

[b.] *Organic Semiconductor Centre, SUPA, School of Physics and Astronomy, University of St. Andrews, St. Andrews, Fife, KY16 9SS, UK.*

Keywords: BODIPY, phenothiazine, PTAA, electrochemistry, DFT, perovskite solar-cell, power conversion efficiency.

E-mail: Graeme.Cooke@glasgow.ac.uk; idws@st-andrews.ac.uk

¶ These authors contributed equally.

1 Materials

All the reagents were purchased from Sigma Aldrich®, Fluorochem®, TCI®, Alfa Aesar®, Acros® or Fisher Scientific® and used as received. Column chromatography was carried out using silica gel (Sigma-Aldrich) 40 – 63 nm 60 Å. The solvent system is specified in each experiment. TLCs were performed using Merck silica gel 60 covered aluminium plates F254. Dry solvents were obtained from Innovative Technology inc. Pure Solv 400-5-MD solvent purification system (activated alumina columns) or Sigma Aldrich®.

2 Synthesis

The synthesis of **PTZ-PTZ-BDP** was accomplished as outlined in **Scheme S1**, in which compounds **2** and **3** were obtained as previously reported [1,2] and then they were used in a Knoevenagel reaction final step.

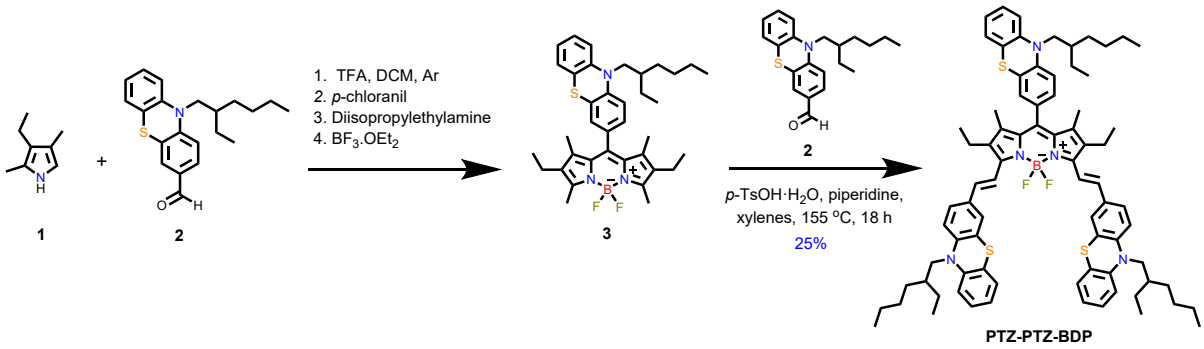

Scheme S1. Synthetic route towards compounds **PTZ-PTZ-BDP**.

Synthesis of PTZ-PTZ-BDP:

To a mixture of compounds **3** (1.574 g, 2.56 mmol) and **2** (3.483 g, 10.3 mmol), *p*-toluenesulfonic acid monohydrate (44 mg, 0.26 mmol) and magnesium sulfate (300 mg) in dry xylenes (30 mL), dry piperidine (2 mL) was added. The resulting mixture was stirred at 155 ^{o}C under argon, for 18 hours. Then, it was allowed to cool to room temperature, filtered and poured into saturated ammonium chloride (100 mL). The organic fraction was extracted with dichloromethane (3 × 80 mL) and the combined organic extracts were washed with water (150 mL) and brine (150 mL), dried over $MgSO_4$ and filtered. After evaporation of the solvent under reduced pressure, the crude material was purified by column chromatography (SiO_2, dichloromethane:petroleum ether; 1:1) to yield **PTZ-PTZ-BDP** as a dark green solid (0.803 g, 25%). Mp: 210–212 °C; ^{1}H NMR (400 MHz, $CDCl_3$) δ 7.65 (d, *J* = 16.7 Hz, 2H), 7.48 (dd, *J* = 8.5, 1.9 Hz, 2H), 7.37 (d, *J* = 1.9 Hz, 2H), 7.23–7.10 (m, 8H), 7.04 (dd, *J* = 6.9, 1.9 Hz, 2H), 6.99–6.85 (m, 9H), 3.82–3.76 (m, 6H), 2.59 (q, *J* = 7.3 Hz, 4H), 2.00–1.92 (m, 3H), 1.51–1.37 (m, 18H), 1.33–1.26 (m, 12H), 1.15 (t, *J* = 7.5 Hz, 6H), 0.94–0.85 (m, 18H); ^{13}C NMR (101 MHz, $CDCl_3$) δ 150.3, 146.1, 146.0, 145.7, 145.5, 138.7, 138.7, 137.1, 134.8, 133.8, 133.4, 132.1, 129.8, 127.8, 127.7, 127.6, 127.4, 127.3, 127.2, 127.2. 126.6, 126.5, 126.1, 125.4, 125.3, 122.8, 122.7, 118.4, 116.5, 116.1, 116.0, 51.4, 51.3, 36.1, 36.0, 31.0, 30.8, 30.8, 29.8, 28.7, 24.1, 23.2, 23.2, 18.5, 14.2, 14.1, 12.0, 12.0, 10.7, 10.6; *m/z* (FAB^{+}) 1255.6547 [M^{+}] ($C_{79}H_{92}{}^{11}BF_2N_5S_3$ requires 1255.6581).

3 NMR Spectra

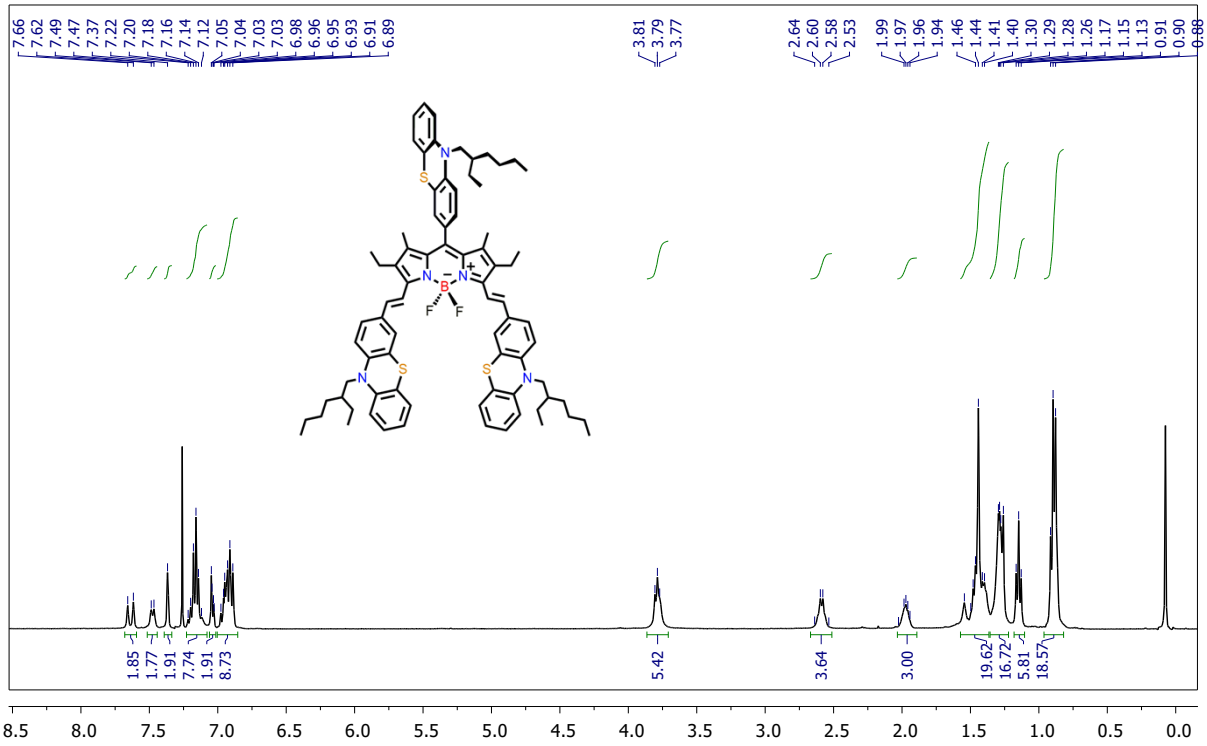

Figure S1: ^{1}H NMR (400 MHz, $CDCl_3$) spectrum of compound **PTZ-PTZ-BDP**.

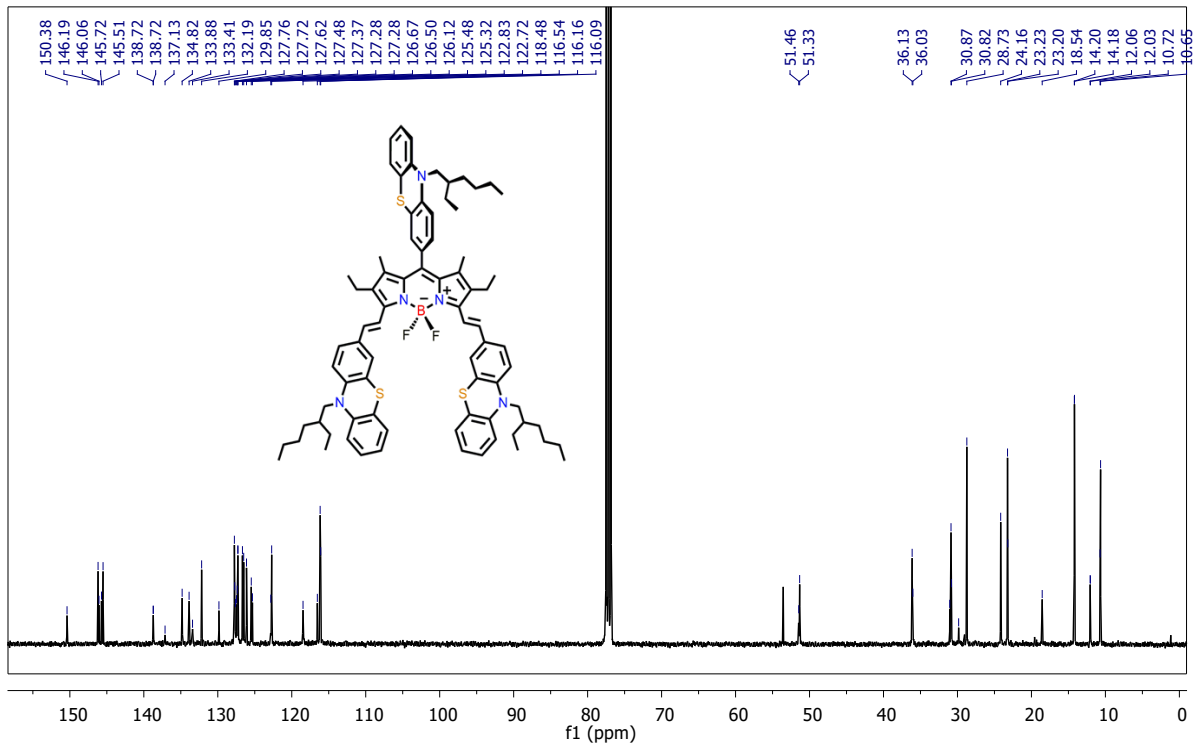

Figure S2: ^{13}C NMR (101 MHz, $CDCl_3$) of compound **PTZ-PTZ-BDP**.

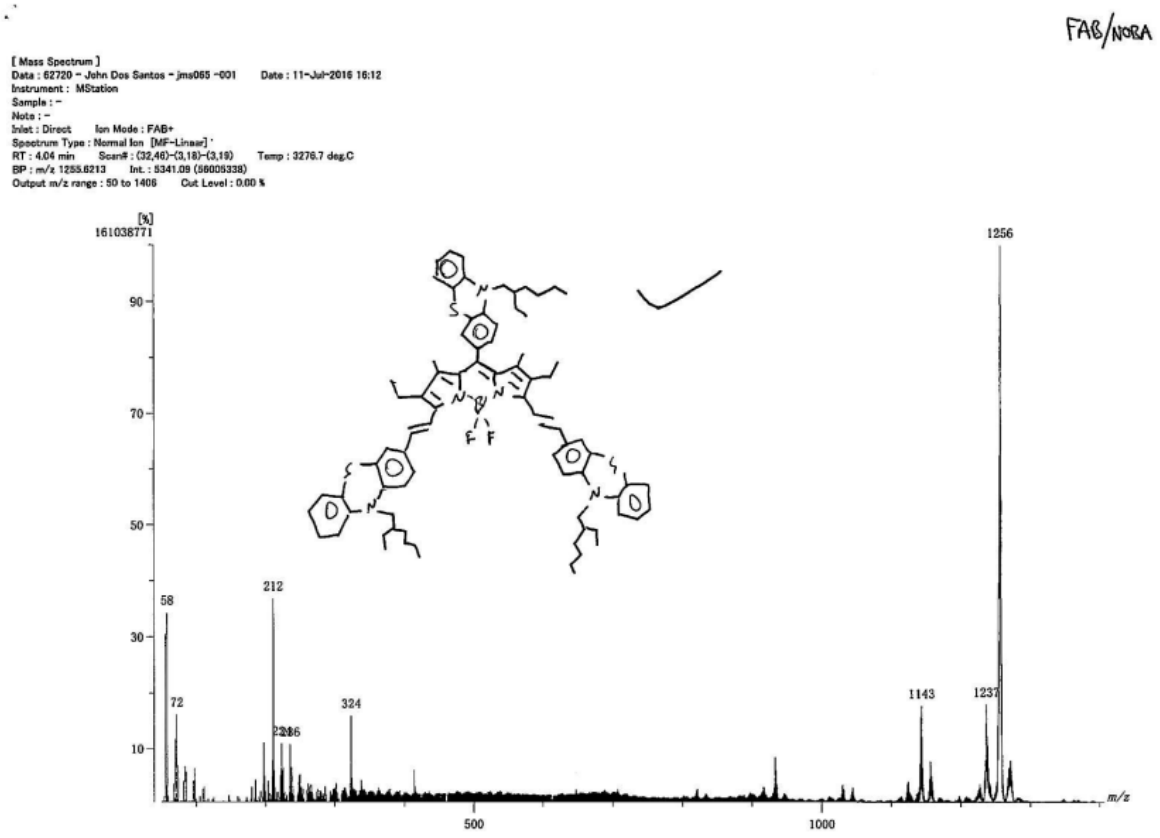

Figure S3: Mass spectrum of **PTZ-PTZ-BDP**.

4 Electrochemistry

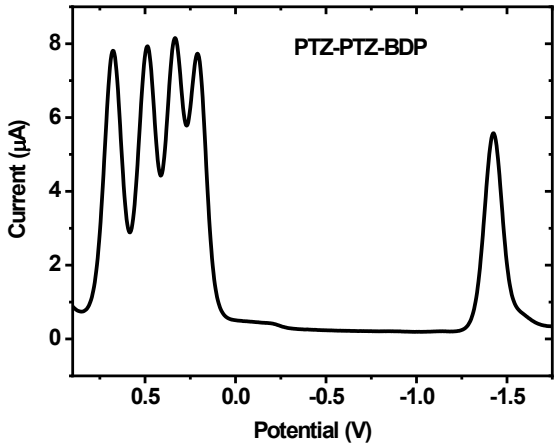

Figure S4. Square wave voltammetry plot of **PTZ- PTZ-BDP**, recorded in DCM (5 x 10^{-4} M), calibrated versus the ferrocene/ferrocenium (Fc/Fc^{+}) redox couple, using $TBA.PF_6$ as electrolyte, a 1.6 mm diameter platinum working electrode, a platinum wire counter electrode and a silver wire pseudo-reference electrode.

4.1 Solid state electrochemistry data for PTZ-PTZ-BDP

A solution of **PTZ-PTZ-BDP** was prepared by dissolving the material in dichloromethane containing TBAB (0.1 M) as an electrolyte. This was then drop-casted onto a glassy carbon electrode and dried at room temperature under a steam of N_2. An Ag/AgCl (sat. KCl) reference electrode and a platinum wire counter electrode were used. All the experiments were conducted in a 0.1 M aqueous KCl solution freshly prepared, which was degassed with N_2 prior each use. Due to the different sensitivities required, oxidation and reduction spectra were run separately, every time using a freshly coated working electrode.

The oxidation and reduction potentials were extrapolated from the square wave voltammetry traces as the onsets of each event and converted to IP and EA, respectively, by the equation:

$$IP\ (eV) = -e\ (4.44\ V + 0.20\ V + E_{ox}) \qquad EA\ (eV) = -e\ (4.44\ V + 0.20\ V + E_{red})$$

Where 4.44 V is the absolute potential of the standard hydrogen electrode (SHE) and 0.20 V is the potential of the Ag/AgCl electrode vs. SHE. The values found for IP and EA are -5.44 eV and -4.14 eV, respectively, with a gap of 1.30 eV.

Cyclic voltammetry

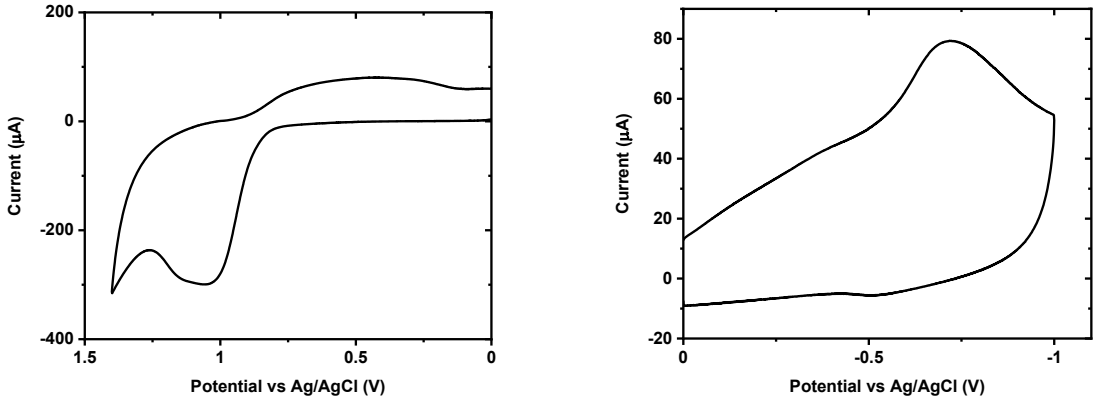

Figure SX. (a) Cyclic voltammetry plot (0 – 1.4 V); scan rate: 0.1 v/s; Sensitivity: 2 x 10^{-5} A/V. (b) Cyclic voltammetry plot (0 – -1.0 V); Scan rate: 0.1 v/s; Sensitivity: 1 x 10^{-6} A/V.

Square wave voltammetry

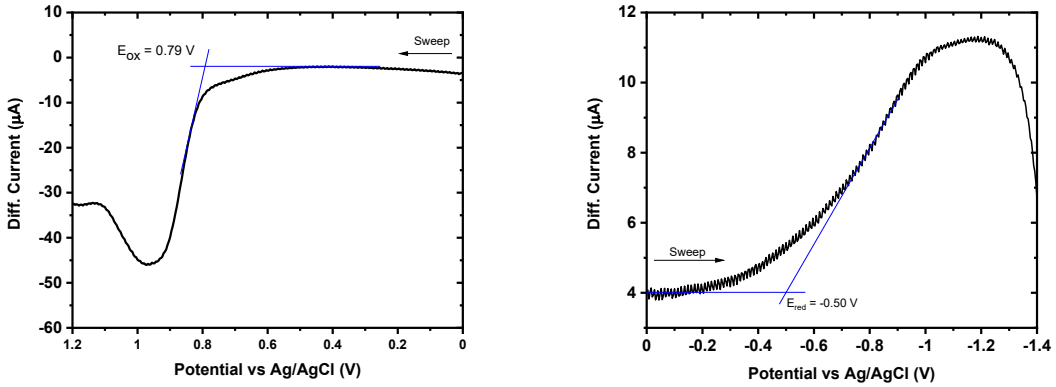

Figure X. (a) Square wave voltammetry plot (0 – 1.2 V); increment: 0.004 V; amplitude: 0.015 V; frequency: 15 Hz; sensitivity: 2 x 10^{-5} A/V. (b) Square wave voltammetry plot (0 – -1.4 V); Increment: 0.004 V; amplitude: 0.015 V; frequency: 15 Hz; sensitivity: 1 x 10^{-6} A/V.

5 DFT

Table S1. Computed energy levels compared with voltammetry data (DFT; B3LYP; 6311G(d,p)).

HOMO	LUMO	E_{gap}	IP (eV)	EA (eV)	E_{fund} (eV)
-4.73	- 2.67	2.05	-5.0	-3.4	1.6

6 General characterization and methodologies

6.1 Chemical structure confirmation:

NMRs were recorded on a Bruker Avance III 400 spectrometer. The ^{1}H and ^{13}C spectra were recorded at 400 and 101 MHz, respectively. The chemical shifts are reported in ppm and coupling constants in Hz as absolute values. Mass spectrometry was obtained from the mass spectrometry service at the University of Glasgow. Melting points (MP) were recorded on a SMP-10 Stuart Scientific melting point machine. Melting points are uncorrected.

6.2 UV/VIS spectroscopy:

UV/VIS spectroscopy was performed using a Perkin Elmer Lambda 25 UV/VIS Spectrometer at room temperature. Solutions were measured in dilute dichloromethane solution ($1x10^{-5}$ M).

6.3 Electrochemical measurements:

Electrochemistry was performed using a CH Instrument Electrochemical Workstation (CHI 440a), Austin, TX, USA. Samples were analysed at 5 x 10^{-4} M concentrations (in dichloromethane) with a scan rate of 0.07 V/s using $TBA[PF]_6$ (0.1 M in corresponding solvent) as the supporting electrolyte. A platinum disk working electrode, a platinum wire counter electrode and a silver wire reference were used for all measurements. The reduction potentials are referred to ferrocene (external reference) with the Fc/Fc^+ redox couple adjusted to 0.0 V.

All the spectroscopic and electrochemical data were processed using Origin Pro 8.5 software suite.

6.4 Theoretical calculations:

DFT calculations were undertaken using the Gaussian 09 software suite.[3] Molecular geometries were initially optimized semi-empirically (PM6) and then re-optimized by DFT [B3LYP/6-311G(d,p) level]. The 2-ethylhexyl chains were replaced by methyl units to facilitate the convergence of the geometry optimizations.

7 Photovoltaic studies

Materials:

All the chemicals used in the present study was used as received without any further purification steps. CH_3NH_3I (MAI) used to prepare the $CH_3NH_3PbI_3$ ($MAPbI_3$) precursor solution was received from Greatcell solar. PbI_2 [99.999% purity] was bought from Alfa Aesar. The SnO_2 solution (CAS 18282-10-5) for the electron transport layer (ETL) was bought from Alfa Aesar and diluted to the volume ratio 1:6.5 in deionized (DI) water prior to spin coating. The materials used for the hole transport material (HTM) solution [2,2',7,7'-Tetrakis[N,N-di(4-

methoxyphenyl)amino]-9,9'-spirobiflourene (Spiro-OMeTAD, >99% purity), 4-*tert*-butyl pyridine (*t*BP, 96% purity), lithium-bis(tri-fluoromethanesulfonyl)imide (Li-TFSI, 99.95% purity) and tris(2-(1H-pyrazol-1-yl)-4-tert-butylpyridine)cobalt(III) tri[bis(trifluoromethane)sulfonimide] (FK 209) were purchased from Ossila, Sigma Aldrich and Greatcell Solar Materials, respectively. The HTM layer of PTAA [Poly[bis(4-phenyl)(2,4,6-trimethylphenyl)amine]] was obtained from the American Dye Sources [ADS260BE, CAS#: 1333317-99-9]. For the p-i-n devices, the $PC_{60}BM$ and poly(4-butyltriphenylamine) (poly-TPD) were purchased from American Dye Source Inc., and poly[(9,9-bis(3'-(N,N-dimethylamino)propyl)-2,7-fluorene)-alt-2,7-(9,9-dioctylfluorene) (PFN) was bought from 1 Materials. Solvents, dimethyl sulfoxide (DMSO, anhydrous, ≥99.9%), N,N-dimethylformamide (DMF, anhydrous, 99.8%), chlorobenzene (anhydrous, 99.8%), acetonitrile (anhydrous, 99.8%), and diethyl ether (anhydrous, ≥99.7%) were purchased from Sigma Aldrich.

Device Fabrication:

For n-i-p devices, patterned indium tin oxide (ITO)-coated glass substrates (glass/ITO with a sheet resistance of 15 Ω cm^{-1}) were sequentially cleaned with sodium dodecyl sulphate (SDS), deionized water, acetone and isopropyl alcohol followed by plasma cleaning for 3 minutes with oxygen plasma in a Plasma Asher. The SnO_2 ETL was spin-coated using 100 µL of SnO_2 solution [diluted to 1:6.5 volume ratio in DI water] at 3000 rpm for 30 seconds, followed by thermal annealing at 150°C for 30 minutes on a hot plate in ambient air conditions inside a laminar flow fume hood. The $MAPbI_3$ precursor solution was prepared using 159 mg of MAI and 461 mg of PbI_2 dissolved in 66 µL of DMSO and 636 µL of DMF and stirred for 1 hour. For the deposition of $MAPbI_3$ perovskite active layer, the precursor solution was spin-coated onto the glass/ITO/SnO_2 substrate at 4000 rpm for 30 s, a diethyl ether (DEE) anti-solvent washing was carried out at the first 7^{th} second of spin-coating process. The spin-coated perovskite films were then annealed under vacuum at 100°C for 1 min followed by 2 mins annealing in ambient N_2 inside a N_2 glovebox.

For the deposition of the HTM, 55 µL of a Spiro-OMeTAD solution [prepared using 72.3 mg of Spiro-OMeTAD, 28.8 µL of *t*BP, 17.5 µL of a Li-TFSI solution (520 mg Li-TFSI in 1 mL acetonitrile) and 29 µL of a FK-209 solution (300 mg FK-209 in 1 mL acetonitrile)] in 1 mL chlorobenzene was spin coated at 4000 rpm for 30 seconds on the perovskite active layer. Before spin coating, the individual solutions for HTL were thoroughly mixed using the vortex

mixer. The PTZ-PTZ-BDP HTLMsolution was prepared by mixing 10 mg of the compound in 1mL of the Chlorobenzene solvent and stirring at 60 ˚C for overnight. The PTAA HTM solution was prepared by mixing 10 mg of the compound in 1mL of the Toluene for 3-4 hours at room temperature. Both PTAA and PTZ-PTZ-BDP HTMs were spin coated at 4000 rpm x 2000 rpm/s x 30 s. To investigate the effect of dopants such as Li-TFSI and *t*BP, they were added to the PTAA and PTZ-PTZ-BDP HTMs in the molar ratio of 0.082 and 0.390 respectively. The same stock solution of Li-TFSI as prepared for the Spiro-OMeTAD was used for the PTAA and PTZ-PTZ-BDP dopants. Thus, the amount of dopants Li-TFSI and *t*BP, added to the 1 mL of PTAA were 1.66 µL and 2.2 µL and 0.34 µL and 0.46 µL to the PTAA and PTZ-PTZ-BDP, respectively. The dopant amount was doubled to explore how the doping influences the corresponding device performances. All the weighing of the HTL and perovskite materials, precursor solution preparation, stirring, perovskite active layer spin coating and the HTM layer depositions were performed inside a nitrogen filled glove box. After the HTM deposition, the perovskite solar cell was then completed by thermally evaporating 100 nm of Au contact. The thickness of the films were measured using Dektak II profilometer (stylus force 6 mg and a measurement range of 6.5 µm).

Characterisation and testing of the solar cells:

After the electrode deposition, the devices were encapsulated with a UV optical adhesive (Norland Optical Adhesive NOA 68) and a glass coverslip. The current-voltage characteristics were determined under an illumination intensity of 100 mW/cm^2 in air using an air mass 1.5 global (AM 1.5G) Sciencetech solar simulator and a Keithley 2400 source-measure unit. The illumination intensity was verified with a calibrated monosilicon detector and a KG-5 filter. The solar cells were applied a bias sweep of from -0.20 V to 1.5 V, with a voltage step of 10 mV and a delay time of 200 ms. The external quantum efficiency (EQE) measurements were performed at zero bias by illuminating the device with monochromatic light supplied from a Xenon arc lamp in combination, with a dual-grating monochromator. The number of photons incident on the sample was calculated for each wavelength by using a silicon photodiode calibrated by the National Physical Laboratory (NPL).

8. Kelvin Probe and APS measurements

Samples for the Kelvin probe and APS measurements were prepared similar to that used for photovoltaic device fabrication (KP Technology APS03 instrument). The Kelvin probe tip has a gold-alloy coating (2 mm diameter) and when used in contact potential difference (CPD) mode, vibrates at 70 Hz at an average height of 1 mm from the sample surface. For recording the ambient photoemission spectrum (APS), the sample was illuminated with a 4-5 mm diameter light spot from a tunable monochromated D2 lamp (4–7 eV). The raw photoemission data were corrected for detector offset; intensity normalized, then processed by a cube root power law. The energy resolution in APS mode is 50-100 meV.

9. Space charge limited current (SCLC) measurement:

The hole only device architecture consists of glass/ITO/ PTZ-PTZ-BDP/Au. The current-voltage curve was measured in the range of 0-6 V using the Fluxim PAIOS measurement platform with Characterization Suite 4.2 software. Hole mobility was calculated from SCLC measurements using the Mott-Gurney equation

Hole mobility was calculated from SCLC measurements using the Mott-Gurney equation:

$$J = \frac{9}{8}\varepsilon_0\varepsilon_r\mu\frac{V^2}{L^3}$$

Where J -current density

V - The applied effective voltage

L - The thickness of the active layer

ε_0 - absolute permittivity

ε_r - relative permittivity (taken as 3)

μ - Hole mobility[4]

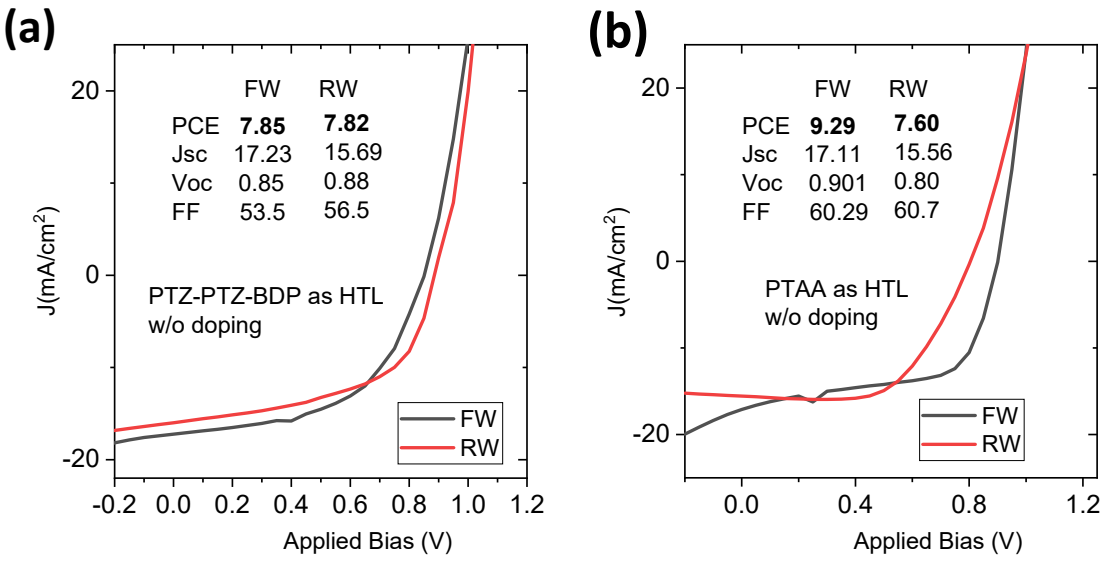

Figure S5: J-V characteristics of the best performing solar cells with the (a) **PTZ-PTZ-BDP** and (b) PTAA as HTM without any dopants.

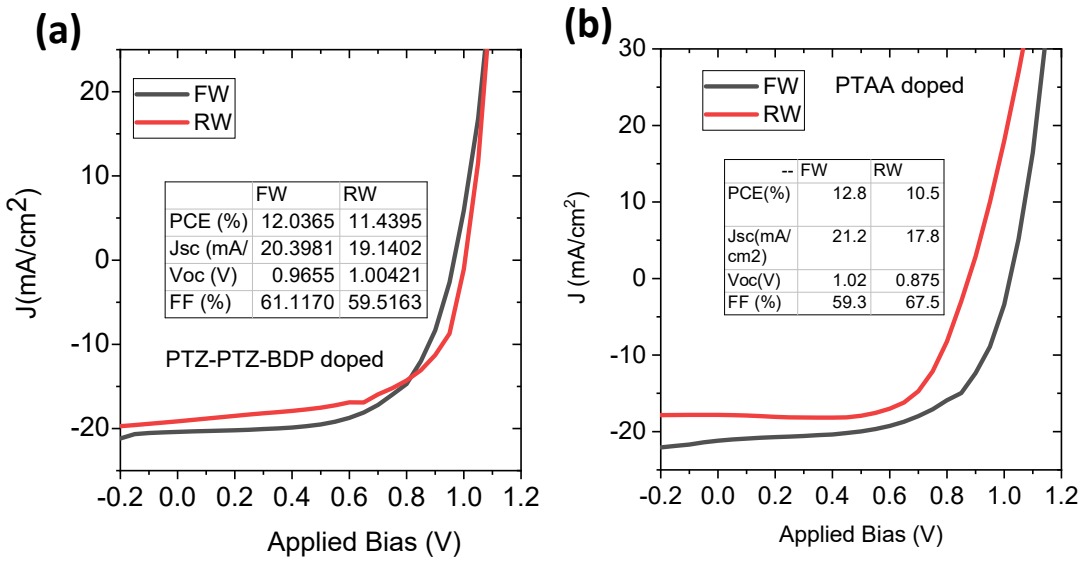

Figure S6: J-V characteristics of the best performing solar cells with the (a) **PTZ-PTZ-BDP** and (b) PTAA as HTLM with dopants of LiTFsi and *t*BP in the ratio of 1:0.082:0.39.

Table S2: Photovoltaic performance parameters of the perovskite solar cells for PTAA and **PTZ-PTZ-BDP** HTM without doping.

HTL (w/o doping)	FW/RW	Jsc (mA/cm^2)	Voc (V)	FF (%)	Rsh (Ohmcm^2)	Rs (Ohmcm^2)	PCE (%) Avg.	PCEmax (%)
PTAA	FW	16.9±1.6	0.836±0.059	55.1±6.6	447±700	1.9±0.9	7.36±1.5	9.3
	RW	13.0±3.7	0.815±0.014	68.5±10.9	636±18	2.56±0.01	7.06±0.77	7.6
PTZ-PTZ-BDP	FW	15.7±1.2	0.761±0.063	50.7±2.2	164±118	1.9±1.3	6.10±1.2	7.85
	RW	14.9±0.7	0.781±0.087	52.2±5.7	268±132	9.3±1.5	6.10±1.2	7.82

Table S3: Photovoltaic performance parameters of the perovskite solar cells for PTAA and **PTZ-PTZ-BDP** as HTMs and with LiTFSi and *t*BP doping.

HTM (doped)	FW/ RW	Jsc (mA/cm^2)	Voc (V)	FF (%)	Rsh (ohm cm^2)	Rs (ohm cm^2)	PCE (%) Avg.	PCEmax (%)
PTZ-PTZ-BDP	FW	18.8±1.3	0.903±0.050	54.9±5.2	326±227	1.1±0.2	9.4±1.9	12.04
	RW	17.3±1.5	0.964±0.024	54.4±3.5	339±162	7.0±2.3	9.10±1.33	11.4
PTAA	FW	18.3±1.9	0.88±0.08	58.9±4.9	305±152	1.5±2.7	9.5±1.8	12.8
	RW	16.0±1.7	0.88±0.03	65.3±2.9	1538±393	5.35±3.5	9.2±1.4	10.5

Table S4: Photovoltaic performance parameters of the doped **PTZ-PTZ-BDP** HTMs (1:0.164:0.78) as a function of their thickness.

Thickness (nm)	FW/ RW	Jsc (mA/cm^2)	Voc (V)	FF (%)	PCE (Avg) (%)	PCEmax (%)
35	FW	18.9±1.8	0.959±0.020	62.3±4.4	11.4±1.6	13.2
	RW	18.2±1.7	1.02±0.02	67.0±8.6	12.4±1.9	14.6
26	FW	18.9±0.52	0.933 ±0.033	61.3±3.4	10.8±0.7	11.7
	RW	17.7±1.3	0.960 ±0.040	62.4±5.2	10.6±1.1	12.8
22	FW	18.4±1.7	0.921±0.071	60.3±6.4	10.3±2.0	12.4
	RW	18.3±0.5	0.988 ±0.029	61.4±6.1	11.1±1.3	12.7

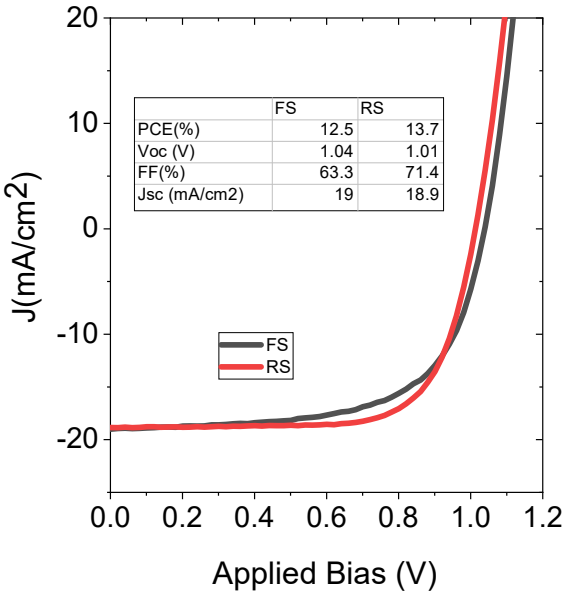

Figure S7: J-V characteristics of the n-i-p $MAPbI_3$ solar cells obtained using Spiro-MeOTAD as the HTM.

Table S5: Photovoltaic performance parameters of the p-i-n perovskite solar cells using **PTZ-PTZ-BDP**+ PFN-P1 as HTMs.

FW/ RW	Jsc (mA/cm^2)	Voc (V)	FF (%)	Rsh (Ωcm^2)	Rs (Ωcm^2)	PCE (Avg) (%)	PCEmax (%)
FW	14.6±0.8	0.775±0.029	41.9±2.9	378.5±150	4.6±1.3	4.74±1.6	5.15
RW	14.8±0.9	0.824±0.023	42.3±4.0	446±162	1.13±0.42	5.13±0.35	5.52

Table S6: Shelf-life stability data of the perovskite solar cells in the n-i-p architecture using **PTZ-PTZ-BDP** and Spiro-MeOTAD as the HTMs.

HTM	Shelf life	FW/RW	Jsc (mA/cm^2)	Voc (V)	FF (%)	PCE (Avg) (%)	PCEmax (%)
PTZ-PTZ-BDP	Day 1	FW	18.9±1.8	0.959±0.020	62.3±4.4	11.4±1.6	13.2
	(Day 1)	RW	18.2±1.7	1.02±0.02	67.0±8.6	12.4±1.9	14.6
	After 6 months	FW	18.5±1.2	0.809 ±0.079	60.4±4.7	9.11±1.7	12.2
		RW	17.5±2.1	0.523 ±0.418	47.4±23.3	6.13±6.1	13.7
Spiro-MeOTAD	Day 1	FW	19.4±2.2	1.06±0.02	47.9±3.3	9.9±1.7	12.5
	(Day 1)	RW	16.8±2.5	1.06±0.03	68.2±1.9	12.1±1.7	14.6
	After 3 months	FW	21.2±1.6	1.02±0.03	49.5±10.5	10.7±2.7	14.5
		RW	15.7±2.9	1.02±0.03	79.6±3.3	12.2±2.1	15.9

References

1 J. Marques dos Santos, L. K. Jagadamma, N. M. Latif, A. Ruseckas, I. D. W. Samuel and G. Cooke, *RSC Advances*, 2019, **9**, 15410–15423.

2 Y. Liu, R. Fujimura, K. Ishida, N. Oya, N. Yoshie, T. Shimura and K. Kuroda, *Journal of Physical Chemistry of Solids*, 2012, **73**, 1136–1145.

3 M. J. Frisch, G. W. Trucks, H. B. Schlegel, G. E. Scuseria, M. A. Robb, J. R. Cheeseman, G. Scalmani, V. Barone, B. Mennucci, G. A. Petersson, H. Nakatsuji, M. Caricato, X. Li, H. P. Hratchian, A. F. Izmaylov, J. Bloino, G. Zheng, J. L. Sonnenberg, M. Hada, M. Ehara, K. Toyota, R. Fukuda, J. Hasegawa, M. Ishida, T. Nakajima, Y. Honda, O. Kitao, H. Nakai, T. Vreven, J. A. Jr. Montgomery, J. E. Peralta, F. Ogliaro, M. Bearpark, J. J. Heyd, E. Brothers, K. N. Kudin, V. N. Staroverov, R. Kobayashi, J. Normand, K. Raghavachari, A. Rendell, J. C. Burant, S. S. Iyengar, J. Tomasi, M. Cossi, N. Rega, J. M. Millam, M. Klene, J. E. Knox, J. B. Cross, V. Bakken, C. Adamo, J. Jaramillo, R. Gomperts, R. E. Stratmann, O. Yazyev, A. J. Austin, R. Cammi, C. Pomelli, J. W. Ochterski, R. L. Martin, K. Morokuma, V. G. Zakrzewski, G. A. Voth, P. Salvador, J. J. Dannenberg, S. Dapprich, A. D. Daniels, Ö. Farkas, J. B. Foresman, J. V. Ortiz, J. Cioslowski and D. J. Fox, 2009.

4 Murray A. Lampert and Peter Mark, *Semiconductor Technique: Current Injection in Solids. Academic Press, New York, 354 pp., Electrical Science series.*, 1970, vol. 170.